PHYSICAL REVIEW D **96,** 114025 (2017)

Cross sections for inelastic meson-meson scattering

Kai Yang,[1] Xiao-Ming Xu,[1] and H. J. Weber[2]
[1]*Department of Physics, Shanghai University, Baoshan, Shanghai 200444, China*
[2]*Department of Physics, University of Virginia, Charlottesville, Virginia 22904, USA*
(Received 29 July 2017; published 26 December 2017)

We study two kinds of inelastic meson-meson scattering. The first kind is inelastic 2-to-2 meson-meson scattering that is governed by quark interchange as well as quark-antiquark annihilation and creation. Cross-section formulas are provided to get unpolarized cross sections for $\pi K \to \rho K^*$ for $I = 1/2$, $\pi K^* \to \rho K$ for $I = 1/2$, $\pi K^* \to \rho K^*$ for $I = 1/2$, and $\rho K \to \rho K^*$ for $I = 1/2$. Near threshold, quark interchange dominates the reactions near the critical temperature. The second kind is 2-to-1 meson-meson scattering with the process that a quark in an initial meson and an antiquark in another initial meson annihilate into a gluon and subsequently the gluon is absorbed by the other antiquark or quark. The transition potential for the process is derived. Four Feynman diagrams at tree level contribute to the 2-to-1 meson-meson scattering. Starting from the S-matrix element, the isospin-averaged unpolarized cross section with transition amplitudes is derived. The cross sections for $\pi\pi \to \rho$ and $\pi K \to K^*$ decrease with increasing temperature.

DOI: 10.1103/PhysRevD.96.114025

I. INTRODUCTION

Meson-meson scattering is an important field in exploring strong interactions. Starting from the chiral perturbation theory Lagrangian, any amplitude for meson-meson scattering is derived to form a perturbative expansion in powers of external momenta and quark masses [1–5]. Depending on what mesons scatter, the calculations of the amplitudes have reached the fourth or sixth power of the external momenta. This expansion is successful in the description of low-energy meson-meson scattering, but cannot describe resonances. In extending chiral perturbation theory to the study of meson-meson scattering beyond the low-energy regime, nonperturbative schemes, for example, the inverse amplitude method, have been proposed. Consequently, resonances can be reproduced and studied within the nonperturbative schemes together with the chiral expansion. Since the elastic phase shifts for $\pi\pi$ scattering and πK scattering can be measured, resonances that contribute to the phase shifts have been studied in the Roy equations [6], the Padé method [7], the inverse amplitude method [4,5,8], the large-N_f expansion [9], the K-matrix method [10], the master formula approach [11], the current algebra unitarization [12], the coupled-channel unitary approaches [13], the N/D method [14], the Bethe-Salpeter approach [15], and the approaches based on effective meson Lagrangians [16–18]. Nevertheless, some isospin channels of the reactions do not involve resonances, and are instead governed, for example, by a quark-interchange process or by annihilation of a quark-antiquark pair and subsequent creation of another quark-antiquark pair. The elastic meson-meson scattering governed by quark interchange is, for example, $\pi\pi$ for $I = 2$ and πK for $I = 3/2$, which have been studied in Ref. [19] in the quark interchange mechanism. The inelastic meson-meson scattering governed by quark interchange is [20,21], for example, $\pi\pi \to \rho\rho$ for $I = 2$, $KK \to K^*K^*$ for $I = 1$, $KK^* \to K^*K^*$ for $I = 1$, $\pi K \to \rho K^*$ for $I = 3/2$, $\pi K^* \to \rho K^*$ for $I = 3/2$, $\rho K \to \rho K^*$ for $I = 3/2$, and $\pi K^* \to \rho K$ for $I = 3/2$. Cross sections for these channels of endothermic reactions have the characteristic that the cross sections rise very rapidly from threshold energies, arrive at maximum values, and decrease rapidly. The inelastic meson-meson scattering governed by quark-antiquark annihilation and creation is [22], for example, $\pi\pi \to \rho\rho$ for $I = 1$, $\pi\pi \to K\bar{K}$ for $I = 1$, $\pi\rho \to K\bar{K}^*$, $\pi\rho \to K^*\bar{K}$, $K\bar{K} \to K^*\bar{K}^*$, and $K\bar{K}^* \to K^*\bar{K}^*$. The cross sections for the endothermic reactions have the characteristic that they may decrease from maximum values very slowly. In Refs. [23,24] isospin-averaged cross sections for $\pi\pi \to K\bar{K}$, $\rho\rho \to K\bar{K}$, $\pi\rho \to K\bar{K}^*$, and $\pi\rho \to K^*\bar{K}$ have been obtained from effective meson Lagrangians via the exchange of either a kaon or a vector kaon between the two initial mesons. The reactions governed by quark interchange or by quark-antiquark annihilation and creation can also be studied by implementing chiral perturbation theory within the nonperturbative schemes. For example, elastic $\pi\pi$ scattering for $I = 2$ and elastic πK scattering for $I = 3/2$ have been studied in Refs. [4–8,13]. The Lagrangian of chiral perturbation theory includes various couplings of pseudoscalar mesons, which establish amplitudes for the scattering. The experimental data of S-wave elastic phase shifts for the scattering are reproduced from the amplitudes by means of the nonperturbative schemes.

In the present work we first study inelastic meson-meson scattering mediated by both quark interchange and quark-antiquark annihilation into a gluon which subsequently creates a quark-antiquark pair. This kind of scattering

includes $\pi K \to \rho K^*$ for $I = 1/2$, $\pi K^* \to \rho K$ for $I = 1/2$, $\pi K^* \to \rho K^*$ for $I = 1/2$, and $\rho K \to \rho K^*$ for $I = 1/2$. Since the four isospin channels of these reactions have not been taken into account in models for ultrarelativistic heavy-ion collisions, our results will be helpful in improving these models. Second, we study the reactions $\pi\pi \to \rho$ and $\pi K \to K^*$ based on quark-antiquark annihilation into a gluon which is further absorbed by a quark or an antiquark. The cross sections we obtain will be compared to experimental data on $\pi\pi \to \rho$ [25] and the estimate derived in Ref. [26] on $\pi K \to K^*$ in vacuum. Since both reactions are important in hadronic matter, we also study their temperature dependence.

Taking the parameter in the Feynman-Hellmann theorem [27] as the quark mass, the theorem can be used to study the dependence of the ground-state hadron mass on the quark mass. The theorem has been recently generalized to unstable states in quantum field theory [28]. Combining the theorem and recent lattice data on the quark-mass dependence of hadron masses, Elvira *et al.* [28] have studied the possible exotic admixture (pentaquarks, tetraquarks, etc.) of hadronic states. They conclude that the ground-state vector mesons are predominantly quark-antiquark states. We thus assume that the ground-state vector mesons are quark-antiquark states.

While Barnes *et al.* [19] study elastic $\pi\pi$ scattering for $I = 2$ and elastic πK scattering for $I = 3/2$, they assume that Born-order quark-interchange diagrams dominate the elastic scattering and that s-channel resonance production and t-channel resonance exchange are not important. While we study inelastic meson-meson scattering in Ref. [22], we assume that diagrams of Born-order quark-antiquark annihilation and creation dominate the inelastic scattering and that the contributions of the annihilation with gluonic excitation into a hybrid meson and the annihilation of a color-singlet quark-antiquark pair into a (virtual) glueball [29] are negligible. In the present work we assume that the diagrams of Born-order quark interchange and the diagrams of Born-order quark-antiquark annihilation and creation dominate the four reactions: $\pi K \to \rho K^*$ for $I = 1/2$, $\pi K^* \to \rho K$ for $I = 1/2$, $\pi K^* \to \rho K^*$ for $I = 1/2$, and $\rho K \to \rho K^*$ for $I = 1/2$.

This paper is organized as follows. In Sec. II we provide cross-section formulas for 2-to-2 meson-meson reactions that are governed not only by quark interchange but also by quark-antiquark annihilation and creation. In Sec. III we derive the formulas of isospin-averaged unpolarized cross sections for 2-to-1 meson-meson reactions. In Sec. IV we derive a transition potential for the process that is a pair of quark-antiquark annihilates into a gluon and subsequently the gluon is absorbed by a quark or an antiquark. Transition amplitudes in the cross section formulas are calculated. In Sec. V numerical cross sections are presented, and relevant discussions are given. In Sec. VI we summarize the present work.

II. CROSS-SECTION FORMULAS FOR 2-TO-2 REACTIONS

Quark interchange leads to the meson-meson scattering processes $A(q_1\bar{q}_1) + B(q_2\bar{q}_2) \to C(q_1\bar{q}_2) + D(q_2\bar{q}_1)$. The scattering may take the prior form where gluon exchange takes place prior to quark interchange or the post form where quark interchange is followed by gluon exchange. The transition amplitude corresponding to the prior form is

$$\begin{aligned}\mathcal{M}_{\rm fi}^{\rm prior} &= \sqrt{2E_A 2E_B 2E_C 2E_D} \\ &\times \int \frac{d^3p_{q_1\bar{q}_2}}{(2\pi)^3}\frac{d^3p_{q_2\bar{q}_1}}{(2\pi)^3}\psi^+_{q_1\bar{q}_2}(\vec{p}_{q_1\bar{q}_2})\psi^+_{q_2\bar{q}_1}(\vec{p}_{q_2\bar{q}_1}) \\ &\times (V_{q_1\bar{q}_2} + V_{\bar{q}_1 q_2} + V_{q_1 q_2} + V_{\bar{q}_1\bar{q}_2}) \\ &\times \psi_{q_1\bar{q}_1}(\vec{p}_{q_1\bar{q}_1})\psi_{q_2\bar{q}_2}(\vec{p}_{q_2\bar{q}_2}), \end{aligned} \tag{1}$$

and the one corresponding to the post form is

$$\begin{aligned}\mathcal{M}_{\rm fi}^{\rm post} &= \sqrt{2E_A 2E_B 2E_C 2E_D} \\ &\times \int \frac{d^3p_{q_1\bar{q}_1}}{(2\pi)^3}\frac{d^3p_{q_2\bar{q}_2}}{(2\pi)^3}\psi^+_{q_1\bar{q}_2}(\vec{p}_{q_1\bar{q}_2})\psi^+_{q_2\bar{q}_1}(\vec{p}_{q_2\bar{q}_1}) \\ &\times (V_{q_1\bar{q}_1} + V_{\bar{q}_2 q_2} + V_{q_1 q_2} + V_{\bar{q}_1\bar{q}_2}) \\ &\times \psi_{q_1\bar{q}_1}(\vec{p}_{q_1\bar{q}_1})\psi_{q_2\bar{q}_2}(\vec{p}_{q_2\bar{q}_2}), \end{aligned} \tag{2}$$

where $\vec{p}_{ab}$ is the relative momentum of constituents a and b; E_A (E_B, E_C, E_D) is the energy of meson A (B, C, D); $\psi_{ab}(\vec{p}_{ab})$ is the mesonic quark-antiquark wave function which is the product of the color wave function, the spin wave function, the flavor wave function, and the relative-motion wave function of constituents a and b; ψ^+_{ab} is the Hermitian conjugate of ψ_{ab}; V_{ab} is the quark potential [30] that is given by perturbative QCD with loop corrections to one-gluon exchange at short distances, that becomes a distance-independent and temperature-dependent potential at long distances, and that has a spin-spin interaction with relativistic modifications. The Fourier transform of the relative-motion part of $\psi_{ab}(\vec{p}_{ab})$ is a solution of the Schrödinger equation with the potential. The meson masses obtained from the Schrödinger equation with the potential at zero temperature are close to the experimental masses of π, ρ, K, K^*, J/ψ, ψ', χ_c, D, D^*, D_s, and D_s^* mesons [31]. Moreover, the experimental data of S-wave phase shifts for the elastic $\pi\pi$ scattering for $I = 2$ in vacuum [32] are reproduced in the Born approximation [30]. In reproducing the experimental meson masses the masses of the up quark, the down quark, the strange quark, and the charm quark are 0.32 GeV, 0.32 GeV, 0.5 GeV, and 1.51 GeV, respectively.

If a quark and an antiquark annihilate into a gluon, this gluon may create a quark-antiquark pair. This process of quark-antiquark annihilation and creation leads to $A(q_1\bar{q}_1) + B(q_2\bar{q}_2) \to C(q_3\bar{q}_1) + D(q_2\bar{q}_4)$ and $A(q_1\bar{q}_1) + B(q_2\bar{q}_2) \to C(q_1\bar{q}_4) + D(q_3\bar{q}_2)$. The transtion amplitude for $A(q_1\bar{q}_1) + B(q_2\bar{q}_2) \to C(q_3\bar{q}_1) + D(q_2\bar{q}_4)$ is

$$\mathcal{M}_{aq_1\bar{q}_2} = \sqrt{2E_A 2E_B 2E_C 2E_D}\int \frac{d^3p_{q_1\bar{q}_1}}{(2\pi)^3}\frac{d^3p_{q_2\bar{q}_2}}{(2\pi)^3} \times \psi^+_{q_3\bar{q}_1}(\vec{p}_{q_3\bar{q}_1})\psi^+_{q_2\bar{q}_4}(\vec{p}_{q_2\bar{q}_4})V_{aq_1\bar{q}_2}(\vec{k}) \times \psi_{q_1\bar{q}_1}(\vec{p}_{q_1\bar{q}_1})\psi_{q_2\bar{q}_2}(\vec{p}_{q_2\bar{q}_2}), \quad (3)$$

and the transition amplitude for $A(q_1\bar{q}_1) + B(q_2\bar{q}_2) \to C(q_1\bar{q}_4) + D(q_3\bar{q}_2)$ is

$$\mathcal{M}_{a\bar{q}_1q_2} = \sqrt{2E_A 2E_B 2E_C 2E_D}\int \frac{d^3p_{q_1\bar{q}_1}}{(2\pi)^3}\frac{d^3p_{q_2\bar{q}_2}}{(2\pi)^3} \times \psi^+_{q_1\bar{q}_4}(\vec{p}_{q_1\bar{q}_4})\psi^+_{q_3\bar{q}_2}(\vec{p}_{q_3\bar{q}_2})V_{a\bar{q}_1q_2}(\vec{k}) \times \psi_{q_1\bar{q}_1}(\vec{p}_{q_1\bar{q}_1})\psi_{q_2\bar{q}_2}(\vec{p}_{q_2\bar{q}_2}), \quad (4)$$

where $\vec{k}$ is the gluon momentum, and $V_{aq_1\bar{q}_2}$ and $V_{a\bar{q}_1q_2}$ are the transition potentials for $q_1 + \bar{q}_2 \to q_3 + \bar{q}_4$ and $\bar{q}_1 + q_2 \to q_3 + \bar{q}_4$, respectively. The transition potentials have been given in Ref. [22]. With the transition amplitudes the experimental data [33] of S-wave $I = 0$ and P-wave $I = 1$ elastic phase shifts for $\pi\pi$ scattering near the threshold energy in vacuum are reproduced.

Meson i ($i = A, B, C, D$) has the angular momentum J_i with its magnetic projection quantum number J_{iz}. In the center-of-mass frame meson A has the momentum $\vec{P}$, meson C has the momentum $\vec{P}'$, and the angle between $\vec{P}$ and $\vec{P}'$ is θ. In hadronic matter the cross section depends on temperature T and $s = (P_A + P_B)^2$, where P_A and P_B are the four-momenta of mesons A and B, respectively. The cross section for the scattering including the quark-interchange process in the prior form as well as the quark-antiquark annihilation and creation is

$$\sigma^{\rm prior}_{\rm unpol}(\sqrt{s}, T) = \frac{1}{(2J_A+1)(2J_B+1)}\frac{1}{32\pi s}\frac{|\vec{P}'(\sqrt{s})|}{|\vec{P}(\sqrt{s})|} \times \int_0^\pi d\theta \sum_{J_{Az}J_{Bz}J_{Cz}J_{Dz}} |\mathcal{M}_{aq_1\bar{q}_2} + \mathcal{M}_{a\bar{q}_1q_2} + \mathcal{M}^{\rm prior}_{\rm fi}|^2 \sin\theta. \quad (5)$$

The cross section for the scattering including the quark-interchange process in the post form as well as the quark-antiquark annihilation and creation is

$$\sigma^{\rm post}_{\rm unpol}(\sqrt{s}, T) = \frac{1}{(2J_A+1)(2J_B+1)}\frac{1}{32\pi s}\frac{|\vec{P}'(\sqrt{s})|}{|\vec{P}(\sqrt{s})|} \times \int_0^\pi d\theta \sum_{J_{Az}J_{Bz}J_{Cz}J_{Dz}} |\mathcal{M}_{aq_1\bar{q}_2} + \mathcal{M}_{a\bar{q}_1q_2} + \mathcal{M}^{\rm post}_{\rm fi}|^2 \sin\theta. \quad (6)$$

The unpolarized cross section is given by

$$\sigma^{\rm unpol}(\sqrt{s}, T) = \frac{1}{2}[\sigma^{\rm prior}_{\rm unpol}(\sqrt{s}, T) + \sigma^{\rm post}_{\rm unpol}(\sqrt{s}, T)]. \quad (7)$$

III. CROSS-SECTION FORMULAS FOR 2-TO-1 REACTIONS

If a quark in meson A and an antiquark in meson B annihilate into a gluon, this gluon may be absorbed by the antiquark in meson A or the quark in meson B. We have four Feynman diagrams shown in Fig. 1 for the reaction $A(q_1\bar{q}_1) + B(q_2\bar{q}_2) \to H(q_2\bar{q}_1 \text{ or } q_1\bar{q}_2)$ where meson H is $q_2\bar{q}_1$ in the two upper diagrams or $q_1\bar{q}_2$ in the two lower diagrams. The S-matrix element for $A + B \to H$ is

$$S_{\rm fi} = \delta_{\rm fi} - 2\pi i\delta(E_{\rm f} - E_{\rm i})(\langle H|V_{{\rm r}q_1\bar{q}_2\bar{q}_1}|A, B\rangle + \langle H|V_{{\rm r}q_1\bar{q}_2q_2}|A, B\rangle + \langle H|V_{{\rm r}q_2\bar{q}_1q_1}|A, B\rangle + \langle H|V_{{\rm r}q_2\bar{q}_1\bar{q}_2}|A, B\rangle), \quad (8)$$

where $E_{\rm i}$ is the total energy of the two initial mesons; $E_{\rm f}$ is the energy of meson H; $V_{{\rm r}q_1\bar{q}_2\bar{q}_1}$ ($V_{{\rm r}q_1\bar{q}_2q_2}$) represents the transition potential for the annihilation of q_1 and $\bar{q}_2$ into a gluon and the subsequent absorption of the gluon by $\bar{q}_1$ in meson A (q_2 in meson B); $V_{{\rm r}q_2\bar{q}_1q_1}$ ($V_{{\rm r}q_2\bar{q}_1\bar{q}_2}$) represents the

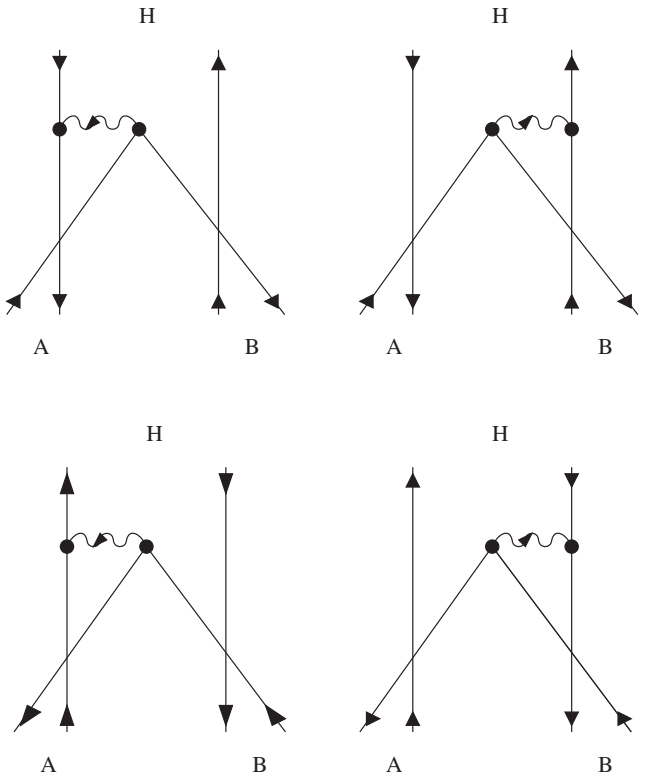

FIG. 1. Reaction $A + B \to H$. Solid lines with up (down) triangles represent quarks (antiquarks). Wavy lines represent gluons.

transition potential for the annihilation of q_2 and $\bar{q}_1$ into a gluon and the subsequent absorption of the gluon by q_1 in meson A ($\bar{q}_2$ in meson B). The wave function of mesons A and B is

$$\psi_{q_1\bar{q}_1,q_2\bar{q}_2} = \frac{e^{i\vec{P}_{q_1\bar{q}_1}\cdot\vec{R}_{q_1\bar{q}_1}}}{\sqrt{V}}\psi_{q_1\bar{q}_1}(\vec{r}_{q_1\bar{q}_1})\frac{e^{i\vec{P}_{q_2\bar{q}_2}\cdot\vec{R}_{q_2\bar{q}_2}}}{\sqrt{V}}\psi_{q_2\bar{q}_2}(\vec{r}_{q_2\bar{q}_2}), \tag{9}$$

where $\vec{P}_{ab}$, $\vec{R}_{ab}$, and $\vec{r}_{ab}$ are the total momentum, the center-of-mass coordinate, and the relative coordinate of a and b, respectively. The wave function of meson H is

$$\psi_{q_2\bar{q}_1} = \frac{e^{i\vec{P}_{q_2\bar{q}_1}\cdot\vec{R}_{q_2\bar{q}_1}}}{\sqrt{V}}\psi_{q_2\bar{q}_1}(\vec{r}_{q_2\bar{q}_1}), \tag{10}$$

corresponding to the two upper diagrams or

$$\psi_{q_1\bar{q}_2} = \frac{e^{i\vec{P}_{q_1\bar{q}_2}\cdot\vec{R}_{q_1\bar{q}_2}}}{\sqrt{V}}\psi_{q_1\bar{q}_2}(\vec{r}_{q_1\bar{q}_2}), \tag{11}$$

corresponding to the two lower diagrams. Every meson wave function is normalized in the volume V.

Now we derive cross-section formulas for $A + B \to H$. For this we denote by $\vec{R}_{\rm total}$ the center-of-mass coordinate of the two initial mesons or the final meson, $\vec{P}_{\rm i}$ ($\vec{P}_{\rm f}$) the total momentum of the two initial mesons (the final meson), $\vec{r}_c$ the position vector of constituent c, and m_c the mass of constituent c. Meson i ($i = A, B, H$) has the mass m_i and the four-momentum $P_i = (E_i, \vec{P}_i)$.

We first consider the two upper diagrams in Fig. 1. Three independent constituent position-vectors are $\vec{r}_{q_1}$, $\vec{r}_{\bar{q}_1}$, and $\vec{r}_{q_2}$. They are related to $\vec{R}_{q_2\bar{q}_1}$, $\vec{r}_{q_1\bar{q}_1}$, and $\vec{r}_{q_2\bar{q}_2}$ by

$$\vec{r}_{q_1} = \vec{R}_{q_2\bar{q}_1} + \frac{m_{\bar{q}_1}}{m_{q_2}+m_{\bar{q}_1}}\vec{r}_{q_1\bar{q}_1} - \frac{m_{q_2}}{m_{q_2}+m_{\bar{q}_1}}\vec{r}_{q_2\bar{q}_2}, \tag{12}$$

$$\vec{r}_{\bar{q}_1} = \vec{R}_{q_2\bar{q}_1} - \frac{m_{q_2}}{m_{q_2}+m_{\bar{q}_1}}\vec{r}_{q_1\bar{q}_1} - \frac{m_{q_2}}{m_{q_2}+m_{\bar{q}_1}}\vec{r}_{q_2\bar{q}_2}, \tag{13}$$

$$\vec{r}_{q_2} = \vec{R}_{q_2\bar{q}_1} + \frac{m_{\bar{q}_1}}{m_{q_2}+m_{\bar{q}_1}}\vec{r}_{q_1\bar{q}_1} + \frac{m_{\bar{q}_1}}{m_{q_2}+m_{\bar{q}_1}}\vec{r}_{q_2\bar{q}_2}, \tag{14}$$

which lead to

$$d\vec{r}_{q_1}d\vec{r}_{\bar{q}_1}d\vec{r}_{q_2} = d\vec{r}_{q_1\bar{q}_1}d\vec{r}_{q_2\bar{q}_2}d\vec{R}_{\rm total}. \tag{15}$$

From the wave functions of the initial and final mesons and the independent position vectors we have for the left upper diagram:

$$\begin{aligned}
&\langle H|V_{{\rm r}q_1\bar{q}_2\bar{q}_1}|A,B\rangle \\
&\quad = \langle q_2\bar{q}_1|V_{{\rm r}q_1\bar{q}_2\bar{q}_1}|q_1\bar{q}_1, q_2\bar{q}_2\rangle \\
&\quad = \int d\vec{r}_{q_1}d\vec{r}_{\bar{q}_1}d\vec{r}_{q_2}\frac{e^{-i\vec{P}_{q_2\bar{q}_1}\cdot\vec{R}_{q_2\bar{q}_1}}}{\sqrt{V}}\psi^+_{q_2\bar{q}_1}(\vec{r}_{q_2\bar{q}_1}) \\
&V_{{\rm r}q_1\bar{q}_2\bar{q}_1}\frac{e^{i\vec{P}_{q_1\bar{q}_1}\cdot\vec{R}_{q_1\bar{q}_1}}}{\sqrt{V}}\psi_{q_1\bar{q}_1}(\vec{r}_{q_1\bar{q}_1})\frac{e^{i\vec{P}_{q_2\bar{q}_2}\cdot\vec{R}_{q_2\bar{q}_2}}}{\sqrt{V}}\psi_{q_2\bar{q}_2}(\vec{r}_{q_2\bar{q}_2}) \\
&\quad = \int d\vec{r}_{q_1\bar{q}_1}d\vec{r}_{q_2\bar{q}_2}d\vec{R}_{\rm total}V^{-\frac{3}{2}}e^{-i\vec{P}_{\rm f}\cdot\vec{R}_{\rm total}}\psi^+_{q_2\bar{q}_1}(\vec{r}_{q_2\bar{q}_1}) \\
&V_{{\rm r}q_1\bar{q}_2\bar{q}_1}\psi_{q_1\bar{q}_1}(\vec{r}_{q_1\bar{q}_1})\psi_{q_2\bar{q}_2}(\vec{r}_{q_2\bar{q}_2})e^{i\vec{P}_{\rm i}\cdot\vec{R}_{\rm total}+i\vec{p}_{q_1\bar{q}_1,q_2\bar{q}_2}\cdot\vec{r}_{q_1\bar{q}_1,q_2\bar{q}_2}} \\
&\quad = (2\pi)^3\delta^3(\vec{P}_{\rm f}-\vec{P}_{\rm i})\frac{\mathcal{M}_{{\rm r}q_1\bar{q}_2\bar{q}_1}}{V^{\frac{3}{2}}\sqrt{2E_A2E_B2E_H}},
\end{aligned} \tag{16}$$

where $\vec{r}_{q_1\bar{q}_1,q_2\bar{q}_2}$ ($\vec{p}_{q_1\bar{q}_1,q_2\bar{q}_2}$) is the relative coordinate (the relative momentum) of $q_1\bar{q}_1$ and $q_2\bar{q}_2$, and the transition amplitude is

$$\begin{aligned}
&\mathcal{M}_{{\rm r}q_1\bar{q}_2\bar{q}_1} \\
&\quad = \sqrt{2E_A2E_B2E_H}\int d\vec{r}_{q_1\bar{q}_1}d\vec{r}_{q_2\bar{q}_2}\psi^+_{q_2\bar{q}_1}(\vec{r}_{q_2\bar{q}_1})V_{{\rm r}q_1\bar{q}_2\bar{q}_1} \\
&\qquad \times\psi_{q_1\bar{q}_1}(\vec{r}_{q_1\bar{q}_1})\psi_{q_2\bar{q}_2}(\vec{r}_{q_2\bar{q}_2})e^{i\vec{p}_{q_1\bar{q}_1,q_2\bar{q}_2}\cdot\vec{r}_{q_1\bar{q}_1,q_2\bar{q}_2}}.
\end{aligned} \tag{17}$$

For the right upper diagram we obtain

$$\begin{aligned}
\langle H|V_{{\rm r}q_1\bar{q}_2q_2}|A,B\rangle &= \langle q_2\bar{q}_1|V_{{\rm r}q_1\bar{q}_2q_2}|q_1\bar{q}_1, q_2\bar{q}_2\rangle \\
&= (2\pi)^3\delta^3(\vec{P}_{\rm f}-\vec{P}_{\rm i})\frac{\mathcal{M}_{{\rm r}q_1\bar{q}_2q_2}}{V^{\frac{3}{2}}\sqrt{2E_A2E_B2E_H}},
\end{aligned} \tag{18}$$

with the transition amplitude

$$\begin{aligned}
&\mathcal{M}_{{\rm r}q_1\bar{q}_2q_2} \\
&\quad = \sqrt{2E_A2E_B2E_H}\int d\vec{r}_{q_1\bar{q}_1}d\vec{r}_{q_2\bar{q}_2}\psi^+_{q_2\bar{q}_1}(\vec{r}_{q_2\bar{q}_1})V_{{\rm r}q_1\bar{q}_2q_2} \\
&\qquad \times\psi_{q_1\bar{q}_1}(\vec{r}_{q_1\bar{q}_1})\psi_{q_2\bar{q}_2}(\vec{r}_{q_2\bar{q}_2})e^{i\vec{p}_{q_1\bar{q}_1,q_2\bar{q}_2}\cdot\vec{r}_{q_1\bar{q}_1,q_2\bar{q}_2}}.
\end{aligned} \tag{19}$$

Next, we consider the two lower diagrams in Fig. 1. The three independent constituent position-vectors are $\vec{r}_{q_1}$, $\vec{r}_{\bar{q}_1}$, and $\vec{r}_{\bar{q}_2}$. They are related to $\vec{R}_{q_1\bar{q}_2}$, $\vec{r}_{q_1\bar{q}_1}$, and $\vec{r}_{q_2\bar{q}_2}$ by

$$\vec{r}_{q_1} = \vec{R}_{q_1\bar{q}_2} + \frac{m_{\bar{q}_2}}{m_{q_1}+m_{\bar{q}_2}}\vec{r}_{q_1\bar{q}_1} + \frac{m_{\bar{q}_2}}{m_{q_1}+m_{\bar{q}_2}}\vec{r}_{q_2\bar{q}_2}, \tag{20}$$

$$\vec{r}_{\bar{q}_1} = \vec{R}_{q_1\bar{q}_2} - \frac{m_{q_1}}{m_{q_1}+m_{\bar{q}_2}}\vec{r}_{q_1\bar{q}_1} + \frac{m_{\bar{q}_2}}{m_{q_1}+m_{\bar{q}_2}}\vec{r}_{q_2\bar{q}_2}, \tag{21}$$

$$\vec{r}_{\bar{q}_2} = \vec{R}_{q_1\bar{q}_2} - \frac{m_{q_1}}{m_{q_1}+m_{\bar{q}_2}}\vec{r}_{q_1\bar{q}_1} - \frac{m_{q_1}}{m_{q_1}+m_{\bar{q}_2}}\vec{r}_{q_2\bar{q}_2}, \tag{22}$$

which lead to

$$d\vec{r}_{q_1} d\vec{r}_{\bar{q}_1} d\vec{r}_{\bar{q}_2} = d\vec{r}_{q_1\bar{q}_1} d\vec{r}_{q_2\bar{q}_2} d\vec{R}_{\rm total}. \quad (23)$$

Using the independent position vectors and Eq. (23), we have for the left lower diagram:

$$\begin{aligned}
&\langle H|V_{{\rm r}q_2\bar{q}_1q_1}|A,B\rangle \\
&\quad = \langle q_1\bar{q}_2|V_{{\rm r}q_2\bar{q}_1q_1}|q_1\bar{q}_1, q_2\bar{q}_2\rangle \\
&\quad = \int d\vec{r}_{q_1} d\vec{r}_{\bar{q}_1} d\vec{r}_{\bar{q}_2} \frac{e^{-i\vec{P}_{\rm f}\cdot\vec{R}_{\rm total}}}{\sqrt{V}} \psi^+_{q_1\bar{q}_2}(\vec{r}_{q_1\bar{q}_2}) \\
&V_{{\rm r}q_2\bar{q}_1q_1} \frac{e^{i\vec{P}_{q_1\bar{q}_1}\cdot\vec{R}_{q_1\bar{q}_1}}}{\sqrt{V}} \psi_{q_1\bar{q}_1}(\vec{r}_{q_1\bar{q}_1}) \frac{e^{i\vec{P}_{q_2\bar{q}_2}\cdot\vec{R}_{q_2\bar{q}_2}}}{\sqrt{V}} \psi_{q_2\bar{q}_2}(\vec{r}_{q_2\bar{q}_2}) \\
&\quad = \int d\vec{r}_{q_1\bar{q}_1} d\vec{r}_{q_2\bar{q}_2} d\vec{R}_{\rm total} V^{-\frac{3}{2}} e^{-i\vec{P}_{\rm f}\cdot\vec{R}_{\rm total}} \psi^+_{q_1\bar{q}_2}(\vec{r}_{q_1\bar{q}_2}) \\
&V_{{\rm r}q_2\bar{q}_1q_1} \psi_{q_1\bar{q}_1}(\vec{r}_{q_1\bar{q}_1}) \psi_{q_2\bar{q}_2}(\vec{r}_{q_2\bar{q}_2}) e^{i\vec{P}_{\rm i}\cdot\vec{R}_{\rm total} + i\vec{p}_{q_1\bar{q}_1,q_2\bar{q}_2}\cdot\vec{r}_{q_1\bar{q}_1,q_2\bar{q}_2}} \\
&\quad = (2\pi)^3\delta^3(\vec{P}_{\rm f} - \vec{P}_{\rm i}) \frac{\mathcal{M}_{{\rm r}q_2\bar{q}_1q_1}}{V^{\frac{3}{2}}\sqrt{2E_A 2E_B 2E_H}}, \quad (24)
\end{aligned}$$

with

$$\begin{aligned}
&\mathcal{M}_{{\rm r}q_2\bar{q}_1q_1} \\
&\quad = \sqrt{2E_A 2E_B 2E_H} \int d\vec{r}_{q_1\bar{q}_1} d\vec{r}_{q_2\bar{q}_2} \psi^+_{q_1\bar{q}_2}(\vec{r}_{q_1\bar{q}_2}) V_{{\rm r}q_2\bar{q}_1q_1} \\
&\qquad \times \psi_{q_1\bar{q}_1}(\vec{r}_{q_1\bar{q}_1}) \psi_{q_2\bar{q}_2}(\vec{r}_{q_2\bar{q}_2}) e^{i\vec{p}_{q_1\bar{q}_1,q_2\bar{q}_2}\cdot\vec{r}_{q_1\bar{q}_1,q_2\bar{q}_2}}. \quad (25)
\end{aligned}$$

For the right lower diagram we obtain

$$\begin{aligned}
\langle H|V_{{\rm r}q_2\bar{q}_1\bar{q}_2}|A,B\rangle &= \langle q_1\bar{q}_2|V_{{\rm r}q_2\bar{q}_1\bar{q}_2}|q_1\bar{q}_1, q_2\bar{q}_2\rangle \\
&= (2\pi)^3\delta^3(\vec{P}_{\rm f} - \vec{P}_{\rm i}) \frac{\mathcal{M}_{{\rm r}q_2\bar{q}_1\bar{q}_2}}{V^{\frac{3}{2}}\sqrt{2E_A 2E_B 2E_H}}, \quad (26)
\end{aligned}$$

with

$$\begin{aligned}
&\mathcal{M}_{{\rm r}q_2\bar{q}_1\bar{q}_2} \\
&\quad = \sqrt{2E_A 2E_B 2E_H} \int d\vec{r}_{q_1\bar{q}_1} d\vec{r}_{q_2\bar{q}_2} \psi^+_{q_1\bar{q}_2}(\vec{r}_{q_1\bar{q}_2}) V_{{\rm r}q_2\bar{q}_1\bar{q}_2} \\
&\qquad \times \psi_{q_1\bar{q}_1}(\vec{r}_{q_1\bar{q}_1}) \psi_{q_2\bar{q}_2}(\vec{r}_{q_2\bar{q}_2}) e^{i\vec{p}_{q_1\bar{q}_1,q_2\bar{q}_2}\cdot\vec{r}_{q_1\bar{q}_1,q_2\bar{q}_2}}. \quad (27)
\end{aligned}$$

We take the Fourier transform of the meson wave functions and the transition potentials:

$$\psi_{q_1\bar{q}_1}(\vec{r}_{q_1\bar{q}_1}) = \int \frac{d^3p_{q_1\bar{q}_1}}{(2\pi)^3} \psi_{q_1\bar{q}_1}(\vec{p}_{q_1\bar{q}_1}) e^{i\vec{p}_{q_1\bar{q}_1}\cdot\vec{r}_{q_1\bar{q}_1}}, \quad (28)$$

$$\psi_{q_2\bar{q}_2}(\vec{r}_{q_2\bar{q}_2}) = \int \frac{d^3p_{q_2\bar{q}_2}}{(2\pi)^3} \psi_{q_2\bar{q}_2}(\vec{p}_{q_2\bar{q}_2}) e^{i\vec{p}_{q_2\bar{q}_2}\cdot\vec{r}_{q_2\bar{q}_2}}, \quad (29)$$

$$\psi_{q_2\bar{q}_1}(\vec{r}_{q_2\bar{q}_1}) = \int \frac{d^3p_{q_2\bar{q}_1}}{(2\pi)^3} \psi_{q_2\bar{q}_1}(\vec{p}_{q_2\bar{q}_1}) e^{i\vec{p}_{q_2\bar{q}_1}\cdot\vec{r}_{q_2\bar{q}_1}}, \quad (30)$$

$$\psi_{q_1\bar{q}_2}(\vec{r}_{q_1\bar{q}_2}) = \int \frac{d^3p_{q_1\bar{q}_2}}{(2\pi)^3} \psi_{q_1\bar{q}_2}(\vec{p}_{q_1\bar{q}_2}) e^{i\vec{p}_{q_1\bar{q}_2}\cdot\vec{r}_{q_1\bar{q}_2}}, \quad (31)$$

$$V_{{\rm r}q_1\bar{q}_2\bar{q}_1}(\vec{r}_{\bar{q}_1} - \vec{r}_{q_1}) = \int \frac{d^3k}{(2\pi)^3} V_{{\rm r}q_1\bar{q}_2\bar{q}_1}(\vec{k}) e^{i\vec{k}\cdot(\vec{r}_{\bar{q}_1} - \vec{r}_{q_1})}, \quad (32)$$

$$V_{{\rm r}q_1\bar{q}_2q_2}(\vec{r}_{q_2} - \vec{r}_{\bar{q}_2}) = \int \frac{d^3k}{(2\pi)^3} V_{{\rm r}q_1\bar{q}_2q_2}(\vec{k}) e^{i\vec{k}\cdot(\vec{r}_{q_2} - \vec{r}_{\bar{q}_2})}, \quad (33)$$

$$V_{{\rm r}q_2\bar{q}_1q_1}(\vec{r}_{q_1} - \vec{r}_{\bar{q}_1}) = \int \frac{d^3k}{(2\pi)^3} V_{{\rm r}q_2\bar{q}_1q_1}(\vec{k}) e^{i\vec{k}\cdot(\vec{r}_{q_1} - \vec{r}_{\bar{q}_1})}, \quad (34)$$

$$V_{{\rm r}q_2\bar{q}_1\bar{q}_2}(\vec{r}_{\bar{q}_2} - \vec{r}_{q_2}) = \int \frac{d^3k}{(2\pi)^3} V_{{\rm r}q_2\bar{q}_1\bar{q}_2}(\vec{k}) e^{i\vec{k}\cdot(\vec{r}_{\bar{q}_2} - \vec{r}_{q_2})}, \quad (35)$$

where $\vec{k}$ is the gluon momentum. The normalizations are $\int d\vec{r}_{ab}\psi^+_{ab}(\vec{r}_{ab})\psi_{ab}(\vec{r}_{ab})=1$ and $\int \frac{d^3p_{ab}}{(2\pi)^3}\psi^+_{ab}(\vec{p}_{ab})\psi_{ab}(\vec{p}_{ab})=1$. Substitute the Fourier transform in Eqs. (17), (19), (25), and (27) to get

$$\begin{aligned}
\mathcal{M}_{{\rm r}q_1\bar{q}_2\bar{q}_1} &= \sqrt{2E_A 2E_B 2E_H} \int \frac{d^3p_{q_1\bar{q}_1}}{(2\pi)^3} \frac{d^3p_{q_2\bar{q}_2}}{(2\pi)^3} \psi^+_{q_2\bar{q}_1}(\vec{p}_{q_2\bar{q}_1}) \\
&\quad \times V_{{\rm r}q_1\bar{q}_2\bar{q}_1}(\vec{k}) \psi_{q_1\bar{q}_1}(\vec{p}_{q_1\bar{q}_1}) \psi_{q_2\bar{q}_2}(\vec{p}_{q_2\bar{q}_2}), \quad (36)
\end{aligned}$$

$$\begin{aligned}
\mathcal{M}_{{\rm r}q_1\bar{q}_2q_2} &= \sqrt{2E_A 2E_B 2E_H} \int \frac{d^3p_{q_1\bar{q}_1}}{(2\pi)^3} \frac{d^3p_{q_2\bar{q}_2}}{(2\pi)^3} \psi^+_{q_2\bar{q}_1}(\vec{p}_{q_2\bar{q}_1}) \\
&\quad \times V_{{\rm r}q_1\bar{q}_2q_2}(\vec{k}) \psi_{q_1\bar{q}_1}(\vec{p}_{q_1\bar{q}_1}) \psi_{q_2\bar{q}_2}(\vec{p}_{q_2\bar{q}_2}), \quad (37)
\end{aligned}$$

$$\begin{aligned}
\mathcal{M}_{{\rm r}q_2\bar{q}_1q_1} &= \sqrt{2E_A 2E_B 2E_H} \int \frac{d^3p_{q_1\bar{q}_1}}{(2\pi)^3} \frac{d^3p_{q_2\bar{q}_2}}{(2\pi)^3} \psi^+_{q_1\bar{q}_2}(\vec{p}_{q_1\bar{q}_2}) \\
&\quad \times V_{{\rm r}q_2\bar{q}_1q_1}(\vec{k}) \psi_{q_1\bar{q}_1}(\vec{p}_{q_1\bar{q}_1}) \psi_{q_2\bar{q}_2}(\vec{p}_{q_2\bar{q}_2}), \quad (38)
\end{aligned}$$

$$\begin{aligned}
\mathcal{M}_{{\rm r}q_2\bar{q}_1\bar{q}_2} &= \sqrt{2E_A 2E_B 2E_H} \int \frac{d^3p_{q_1\bar{q}_1}}{(2\pi)^3} \frac{d^3p_{q_2\bar{q}_2}}{(2\pi)^3} \psi^+_{q_1\bar{q}_2}(\vec{p}_{q_1\bar{q}_2}) \\
&\quad \times V_{{\rm r}q_2\bar{q}_1\bar{q}_2}(\vec{k}) \psi_{q_1\bar{q}_1}(\vec{p}_{q_1\bar{q}_1}) \psi_{q_2\bar{q}_2}(\vec{p}_{q_2\bar{q}_2}). \quad (39)
\end{aligned}$$

The unpolarized cross section for $A+B\to H$ is

$$\sigma^{\rm unpol}=\frac{\pi\delta(E_{\rm f}-E_{\rm i})}{4\sqrt{(P_A\cdot P_B)^2-m_A^2m_B^2}E_H}\frac{1}{(2J_A+1)(2J_B+1)}\times\sum_{J_{Az}J_{Bz}J_{Hz}}|\mathcal{M}_{{\rm r}q_1\bar{q}_2\bar{q}_1}+\mathcal{M}_{{\rm r}q_1\bar{q}_2q_2}+\mathcal{M}_{{\rm r}q_2\bar{q}_1q_1}+\mathcal{M}_{{\rm r}q_2\bar{q}_1\bar{q}_2}|^2. \tag{40}$$

In the center-of-mass frame of the two initial mesons $E_{\rm f}=m_H$ and $E_{\rm i}=\sqrt{s}$. Then, $\delta(E_{\rm f}-E_{\rm i})=\delta(E_{\rm i}-E_{\rm f})=\delta(\sqrt{s}-m_H)$. The experimental cross sections of $\pi\pi\to\rho$ are large but finite. Since $\delta(x)=\lim_{h\to0}\frac{1}{h\sqrt{\pi}}\exp(-\frac{x^2}{h^2})$, we approximate $\delta(\sqrt{s}-m_H)$ by $\frac{1}{h\sqrt{\pi}}\exp(-\frac{(\sqrt{s}-m_H)^2}{h^2})$ with a small value of h to mimic the experimental data. Substituting the relation,

$$(P_A\cdot P_B)^2-m_A^2m_B^2=\frac{1}{4}[s-(m_A+m_B)^2][s-(m_A-m_B)^2], \tag{41}$$

in Eq. (40), we get the unpolarized cross section,

$$\sigma^{\rm unpol}=\frac{\sqrt{\pi}\exp(-\frac{(\sqrt{s}-m_H)^2}{h^2})}{2h\sqrt{[s-(m_A+m_B)^2][s-(m_A-m_B)^2]}E_H}\times\frac{1}{(2J_A+1)(2J_B+1)}\times\sum_{J_{Az}J_{Bz}J_{Hz}}|\mathcal{M}_{{\rm r}q_1\bar{q}_2\bar{q}_1}+\mathcal{M}_{{\rm r}q_1\bar{q}_2q_2}+\mathcal{M}_{{\rm r}q_2\bar{q}_1q_1}+\mathcal{M}_{{\rm r}q_2\bar{q}_1\bar{q}_2}|^2, \tag{42}$$

with $\sqrt{s}=m_H$. Let I_A (I_B, I_H) be the isospin of meson A (B, H). The isospin-averaged unpolarized cross section for $A+B\to H$ is

$$\sigma^{\rm un}=\frac{2I_H+1}{(2I_A+1)(2I_B+1)}\sigma^{\rm unpol}. \tag{43}$$

IV. TRANSITION POTENTIAL AND TRANSITION AMPLITUDE

The reaction $A+B\to H$ involves quark-antiquark annihilation into a gluon and subsequent gluon absorption by a quark or an antiquark. This process is shown in Fig. 2 where the left diagram indicates $q'(p_1)+q(p_2)+\bar{q}(-p_3)\to q'(p_1')$ and the right diagram indicates $\bar{q}'(-p_1)+q(p_2)+\bar{q}(-p_3)\to\bar{q}'(-p_1')$. The left diagram has been used to study $p\bar{p}$ annihilation into two mesons [34]. According to the Feynman rules in QCD [35], the amplitude for the left diagram in Fig. 2 is written as

$$\mathcal{M}_{{\rm r}q\bar{q}q'}=\frac{{g_s}^2}{k^2}\bar{\psi}_{q'}(\vec{p}_1',s_{q'z}')\gamma_\tau T^e\psi_{q'}(\vec{p}_1,s_{q'z})\times\bar{\psi}_{\bar{q}}(\vec{p}_3,s_{\bar{q}z})\gamma^\tau T^e\psi_q(\vec{p}_2,s_{qz}), \tag{44}$$

where g_s is the gauge coupling constant; the gluon has the four-momentum k, the color index e, and the space-time index τ; T^e ($e=1,\ldots,8$) are the $SU(3)$ color generators; γ^τ are the Dirac matrices; repeated color and space-time indices (e and τ) are summed. The quark spinors $[\psi_{q'}(\vec{p}_1,s_{q'z})$, $\psi_{q'}(\vec{p}_1',s_{q'z}')$, $\psi_q(\vec{p}_2,s_{qz})]$ and the antiquark spinor $[\psi_{\bar{q}}(\vec{p}_3,s_{\bar{q}z})]$ are given in a familiar way [22,36] by

$$\psi_q(\vec{p}_2,s_{qz})=\begin{pmatrix}G_2(\vec{p}_2)\\ \frac{\vec{\sigma}\cdot\vec{p}_2}{2m_q}G_2(\vec{p}_2)\end{pmatrix}\chi_{s_{qz}}, \tag{45}$$

$$\psi_{\bar{q}}(\vec{p}_3,s_{\bar{q}z})=\begin{pmatrix}\frac{\vec{\sigma}\cdot\vec{p}_3}{2m_{\bar{q}}}G_3(\vec{p}_3)\\ G_3(\vec{p}_3)\end{pmatrix}\chi_{s_{\bar{q}z}}, \tag{46}$$

$$\psi_{q'}(\vec{p}_1,s_{q'z})=\begin{pmatrix}G_1(\vec{p}_1)\\ \frac{\vec{\sigma}\cdot\vec{p}_1}{2m_{q'}}G_1(\vec{p}_1)\end{pmatrix}\chi_{s_{q'z}}, \tag{47}$$

$$\psi_{q'}(\vec{p}_1',s_{q'z}')=\begin{pmatrix}G_1'(\vec{p}_1')\\ \frac{\vec{\sigma}\cdot\vec{p}_1'}{2m_{q'}}G_1'(\vec{p}_1')\end{pmatrix}\chi_{s_{q'z}'}, \tag{48}$$

where $\vec{\sigma}$ are the Pauli matrices, $\chi_{s_{qz}}$, $\chi_{s_{\bar{q}z}}$, $\chi_{s_{q'z}}$, and $\chi_{s_{q'z}'}$ are the spin wave functions with the magnetic projection quantum numbers, s_{qz}, $s_{\bar{q}z}$, $s_{q'z}$, and $s_{q'z}'$, of the quark or antiquark spin, respectively. The amplitude for the right diagram in Fig. 2 is,

$$\mathcal{M}_{{\rm r}q\bar{q}\bar{q}'}=-\frac{{g_s}^2}{k^2}\bar{\psi}_{\bar{q}'}(\vec{p}_1,s_{\bar{q}'z})\gamma_\tau T^e\psi_{\bar{q}'}(\vec{p}_1',s_{\bar{q}'z}')\times\bar{\psi}_{\bar{q}}(\vec{p}_3,s_{\bar{q}z})\gamma^\tau T^e\psi_q(\vec{p}_2,s_{qz}), \tag{49}$$

where the antiquark spinors, $\psi_{\bar{q}'}(\vec{p}_1,s_{\bar{q}'z})$ and $\psi_{\bar{q}'}(\vec{p}_1',s_{\bar{q}'z}')$, are given by

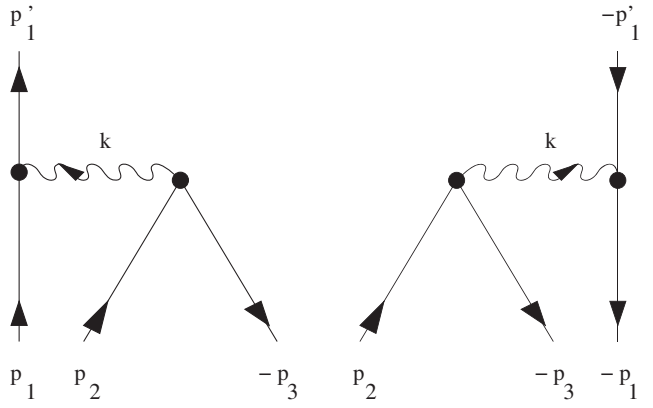

FIG. 2. Left diagram with $q'(p_1)+q(p_2)+\bar{q}(-p_3)\to q'(p_1')$ and right diagram with $\bar{q}'(-p_1)+q(p_2)+\bar{q}(-p_3)\to\bar{q}'(-p_1')$.

$$\psi_{\bar{q}'}(\vec{p}_1, s_{\bar{q}'z}) = \begin{pmatrix} \frac{\vec{\sigma}\cdot\vec{p}_1}{2m_{\bar{q}'}} G_1(\vec{p}_1) \\ G_1(\vec{p}_1) \end{pmatrix} \chi_{s_{\bar{q}'z}}, \tag{50}$$

$$\psi_{\bar{q}'}(\vec{p}'_1, s'_{\bar{q}'z}) = \begin{pmatrix} \frac{\vec{\sigma}\cdot\vec{p}'_1}{2m_{\bar{q}'}} G'_1(\vec{p}'_1) \\ G'_1(\vec{p}'_1) \end{pmatrix} \chi_{s'_{\bar{q}'z}}, \tag{51}$$

where $\chi_{s_{\bar{q}'z}}$ and $\chi_{s'_{\bar{q}'z}}$ are the spin wave functions with the magnetic projection quantum numbers, $s_{\bar{q}'z}$ and $s'_{\bar{q}'z}$, of the antiquark spin, respectively. Keeping such terms to order of the inverse of the quark mass, we get

$$\mathcal{M}_{\mathrm{r}q\bar{q}q'} = \frac{g_s^2}{k^2}\chi^+_{s'_{q'z}}\chi^+_{s_{\bar{q}z}} T^e T^e G'_1(\vec{p}'_1) G_3(\vec{p}_3)\left[\frac{\vec{\sigma}(32)\cdot\vec{k}}{2m_q} - \frac{\vec{\sigma}(1)\cdot\vec{\sigma}(32)\vec{\sigma}(1)\cdot\vec{p}_1 + \vec{\sigma}(1)\cdot\vec{p}'_1\vec{\sigma}(1)\cdot\vec{\sigma}(32)}{2m_{q'}}\right] \times G_1(\vec{p}_1) G_2(\vec{p}_2)\chi_{s_{q'z}}\chi_{s_{qz}}, \tag{52}$$

$$\mathcal{M}_{\mathrm{r}q\bar{q}\bar{q}'} = -\frac{g_s^2}{k^2}\chi^+_{s_{\bar{q}'z}}\chi^+_{s_{\bar{q}z}} T^e T^e G_1(\vec{p}_1) G_3(\vec{p}_3)\left[\frac{\vec{\sigma}(32)\cdot\vec{k}}{2m_q} - \frac{\vec{\sigma}(1)\cdot\vec{p}_1\vec{\sigma}(1)\cdot\vec{\sigma}(32) + \vec{\sigma}(1)\cdot\vec{\sigma}(32)\vec{\sigma}(1)\cdot\vec{p}'_1}{2m_{\bar{q}'}}\right] \times G'_1(\vec{p}'_1) G_2(\vec{p}_2)\chi_{s'_{\bar{q}'z}}\chi_{s_{qz}}. \tag{53}$$

Since $T^e T^e = \frac{\vec{\lambda}(1)}{2}\cdot\frac{\vec{\lambda}(32)}{2}$ with $\vec{\lambda}$ being the Gell-Mann matrices, we obtain the transition potential for $q'(p_1) + q(p_2) + \bar{q}(-p_3) \to q'(p'_1)$,

$$V_{\mathrm{r}q\bar{q}q'}(\vec{k}) = \frac{\vec{\lambda}(1)}{2}\cdot\frac{\vec{\lambda}(32)}{2}\frac{g_s^2}{k^2}\left(\frac{\vec{\sigma}(32)\cdot\vec{k}}{2m_q} - \frac{\vec{\sigma}(1)\cdot\vec{\sigma}(32)\vec{\sigma}(1)\cdot\vec{p}_1 + \vec{\sigma}(1)\cdot\vec{p}'_1\vec{\sigma}(1)\cdot\vec{\sigma}(32)}{2m_{q'}}\right), \tag{54}$$

and the transition potential for $\bar{q}'(-p_1) + q(p_2) + \bar{q}(-p_3) \to \bar{q}'(-p'_1)$,

$$V_{\mathrm{r}q\bar{q}\bar{q}'}(\vec{k}) = -\frac{\vec{\lambda}(1)}{2}\cdot\frac{\vec{\lambda}(32)}{2}\frac{g_s^2}{k^2}\left(\frac{\vec{\sigma}(32)\cdot\vec{k}}{2m_q} - \frac{\vec{\sigma}(1)\cdot\vec{p}_1\vec{\sigma}(1)\cdot\vec{\sigma}(32) + \vec{\sigma}(1)\cdot\vec{\sigma}(32)\vec{\sigma}(1)\cdot\vec{p}'_1}{2m_{\bar{q}'}}\right). \tag{55}$$

In Eqs. (54) and (55), $\vec{\lambda}(32)$ [$\vec{\sigma}(32)$] mean that they have matrix elements between the color (spin) wave functions of the initial antiquark and the initial quark. In Eq. (54), $\vec{\lambda}(1)$ [$\vec{\sigma}(1)$] mean that they have matrix elements between the color (spin) wave functions of the final quark and the initial quark. In Eq. (55), $\vec{\lambda}(1)$ [$\vec{\sigma}(1)$] mean that they have matrix elements between the color (spin) wave functions of the initial antiquark and the final antiquark.

Starting from the quark and antiquark spinors and the gluon-quark vertices with the Dirac matrices, the amplitude for the left or right diagram in Fig. 2 is proportional to the product of the transition potential and the nonrelativistic quark and antiquark wave functions [$G_1(\vec{p}_1)$, $G_2(\vec{p}_2)$, $G_3(\vec{p}_3)$, $G'_1(\vec{p}'_1)$] in Eqs. (52) and (53). Only in obtaining the transition potential we use the quark and antiquark spinors. Because the nonrelativistic wave functions appear in Eqs. (52) and (53), we proceed to get the S-matrix element in Sec. III. In the nonrelativistic framework the product of the nonrelativistic quark and antiquark wave functions in a meson is rewritten as the product of the quark-antiquark relative-motion wave function and the center-of-mass motion wave function as seen in Eqs. (9)–(11). Normalization in the volume V should be given to the wave functions of meson H in Eq. (10) or (11), meson A, and meson B in Eq. (9).

The wave function of mesons A and B is

$$\psi_{AB} = \phi_{A\,\mathrm{rel}}\phi_{B\,\mathrm{rel}}\phi_{A\,\mathrm{color}}\phi_{B\,\mathrm{color}}\chi_{S_A S_{Az}}\chi_{S_B S_{Bz}}\varphi_{AB\,\mathrm{flavor}}, \tag{56}$$

and the wave function of meson H is

$$\psi_H = \phi_{H\,\mathrm{rel}}\phi_{H\,\mathrm{color}}\chi_{S_H S_{Hz}}\phi_{H\,\mathrm{flavor}}, \tag{57}$$

where $\psi_{AB} = \psi_{q_1\bar{q}_1}\psi_{q_2\bar{q}_2}$; $\psi_H = \psi_{q_2\bar{q}_1} = \psi_{q_1\bar{q}_2}$; $\phi_{A\,\mathrm{rel}}$ ($\phi_{B\,\mathrm{rel}}$, $\phi_{H\,\mathrm{rel}}$), $\phi_{A\,\mathrm{color}}$ ($\phi_{B\,\mathrm{color}}$, $\phi_{H\,\mathrm{color}}$), and $\chi_{S_A S_{Az}}$ ($\chi_{S_B S_{Bz}}$, $\chi_{S_H S_{Hz}}$) are the quark-antiquark relative-motion wave function, the color wave function, and the spin wave function of meson A (B, H), respectively; $\phi_{H\,\mathrm{flavor}}$ is the flavor wave function of meson H. The flavor wave function $\varphi_{AB\,\mathrm{flavor}}$ of mesons A and B possesses the same isospin as meson H. The spin of meson A (B, H) is S_A (S_B, S_H) with its magnetic projection quantum number S_{Az} (S_{Bz}, S_{Hz}). The transition amplitudes include color, spin, and flavor matrix elements. The color matrix element is $-\frac{4}{3\sqrt{3}}$, $\frac{4}{3\sqrt{3}}$, $\frac{4}{3\sqrt{3}}$, and $-\frac{4}{3\sqrt{3}}$ for the left upper diagram, the right upper

TABLE I. Spin matrix elements in $\mathcal{M}_{\mathrm{r}q_1\bar{q}_2\bar{q}_1}$ and $\mathcal{M}_{\mathrm{r}q_1\bar{q}_2q_2}$. The initial spin state is $\phi_{\mathrm{iss}}=\chi_{S_AS_{Az}}\chi_{S_BS_{Bz}}$, and the final spin state $\phi_{\mathrm{fss}}=\chi_{S_HS_{Hz}}$. The second to fourth columns correspond to $\mathcal{M}_{\mathrm{r}q_1\bar{q}_2\bar{q}_1}$, and the fifth to seventh columns $\mathcal{M}_{\mathrm{r}q_1\bar{q}_2q_2}$.

S_{Az}	0	0	0	0	0	0
S_{Bz}	0	0	0	0	0	0
S_{Hz}	−1	0	1	−1	0	1
$\phi^+_{\mathrm{fss}}\phi_{\mathrm{iss}}$	$-\frac{1}{2}$	0	$-\frac{1}{2}$	$-\frac{1}{2}$	0	$-\frac{1}{2}$
$\phi^+_{\mathrm{fss}}\sigma_1(32)\phi_{\mathrm{iss}}$	0	$\frac{1}{\sqrt{2}}$	0	0	$\frac{1}{\sqrt{2}}$	0
$\phi^+_{\mathrm{fss}}\sigma_2(32)\phi_{\mathrm{iss}}$	0	0	0	0	0	0
$\phi^+_{\mathrm{fss}}\sigma_3(32)\phi_{\mathrm{iss}}$	$-\frac{1}{2}$	0	$\frac{1}{2}$	$-\frac{1}{2}$	0	$\frac{1}{2}$
$\phi^+_{\mathrm{fss}}\sigma_1(1)\phi_{\mathrm{iss}}$	0	$-\frac{1}{\sqrt{2}}$	0	0	$-\frac{1}{\sqrt{2}}$	0
$\phi^+_{\mathrm{fss}}\sigma_2(1)\phi_{\mathrm{iss}}$	0	0	0	0	0	0
$\phi^+_{\mathrm{fss}}\sigma_3(1)\phi_{\mathrm{iss}}$	$\frac{1}{2}$	0	$-\frac{1}{2}$	$\frac{1}{2}$	0	$-\frac{1}{2}$
$\phi^+_{\mathrm{fss}}\sigma_1(32)\sigma_1(1)\phi_{\mathrm{iss}}$	$\frac{1}{2}$	0	$\frac{1}{2}$	$\frac{1}{2}$	0	$\frac{1}{2}$
$\phi^+_{\mathrm{fss}}\sigma_1(32)\sigma_2(1)\phi_{\mathrm{iss}}$	$-\frac{1}{2}i$	0	$\frac{1}{2}i$	$\frac{1}{2}i$	0	$-\frac{1}{2}i$
$\phi^+_{\mathrm{fss}}\sigma_1(32)\sigma_3(1)\phi_{\mathrm{iss}}$	0	0	0	0	0	0
$\phi^+_{\mathrm{fss}}\sigma_2(32)\sigma_1(1)\phi_{\mathrm{iss}}$	$-\frac{1}{2}i$	0	$\frac{1}{2}i$	$\frac{1}{2}i$	0	$-\frac{1}{2}i$
$\phi^+_{\mathrm{fss}}\sigma_2(32)\sigma_2(1)\phi_{\mathrm{iss}}$	$-\frac{1}{2}$	0	$-\frac{1}{2}$	$-\frac{1}{2}$	0	$-\frac{1}{2}$
$\phi^+_{\mathrm{fss}}\sigma_2(32)\sigma_3(1)\phi_{\mathrm{iss}}$	0	$-\frac{1}{\sqrt{2}}i$	0	0	$\frac{1}{\sqrt{2}}i$	0
$\phi^+_{\mathrm{fss}}\sigma_3(32)\sigma_1(1)\phi_{\mathrm{iss}}$	0	0	0	0	0	0
$\phi^+_{\mathrm{fss}}\sigma_3(32)\sigma_2(1)\phi_{\mathrm{iss}}$	0	$-\frac{1}{\sqrt{2}}i$	0	0	$\frac{1}{\sqrt{2}}i$	0
$\phi^+_{\mathrm{fss}}\sigma_3(32)\sigma_3(1)\phi_{\mathrm{iss}}$	$\frac{1}{2}$	0	$\frac{1}{2}$	$\frac{1}{2}$	0	$\frac{1}{2}$

diagram, the left lower diagram, and the right lower diagram, respectively. The spin matrix elements in $\mathcal{M}_{\mathrm{r}q_1\bar{q}_2\bar{q}_1}$ and $\mathcal{M}_{\mathrm{r}q_1\bar{q}_2q_2}$ are listed in Table I. The spin matrix elements in $\mathcal{M}_{\mathrm{r}\bar{q}_1q_2q_1}$ and $\mathcal{M}_{\mathrm{r}\bar{q}_1q_2\bar{q}_2}$ equal the ones in $\mathcal{M}_{\mathrm{r}q_1\bar{q}_2q_2}$ and $\mathcal{M}_{\mathrm{r}q_1\bar{q}_2\bar{q}_1}$, respectively. The flavor matrix element of $\pi\pi\to\rho$ ($\pi K\to K^*$) is 1 (0) for the two upper diagrams and -1 ($-\frac{\sqrt{6}}{2}$) for the two lower diagrams.

V. NUMERICAL CROSS SECTIONS AND DISCUSSIONS

We consider the following inelastic meson-meson scattering processes that are governed not only by quark interchange but also by quark-antiquark annihilation and creation:

$$I=1/2\pi K^*\to\rho K,\qquad I=1/2\pi K^*\to\rho K^*,$$
$$I=1/2\pi K\to\rho K^*,\qquad I=1/2\rho K\to\rho K^*.$$

The flavor matrix elements of the four channels are $-1/2$ in $\mathcal{M}_{\mathrm{fi}}^{\mathrm{prior}}$ and $\mathcal{M}_{\mathrm{fi}}^{\mathrm{post}}$, 0 in $\mathcal{M}_{\mathrm{a}q_1\bar{q}_2}$, and 3/2 in $\mathcal{M}_{\mathrm{a}\bar{q}_1q_2}$. According to Eq. (7) we calculate unpolarized cross sections at the six temperatures $T/T_{\mathrm{c}}=0$, 0.65, 0.75, 0.85, 0.9, and 0.95, where T_{c} is the critical temperature and equals 0.175 GeV. In Figs. 3–6 we plot the unpolarized cross sections for the four channels of the reactions. A quark-gluon plasma is produced in high-energy Au-Au collisions at the Relativistic Heavy Ion Collider. The quark-gluon plasma is not a phase of chiral symmetry restoration, but is a deconfined phase. The Au-Au collisions undergo the phase transition between confinement and deconfinement. The transition temperature T_{c} measured from Au-Au collisions is 0.175 GeV [37]. This is consistent with the prediction of the lattice gauge calculations in Ref. [38].

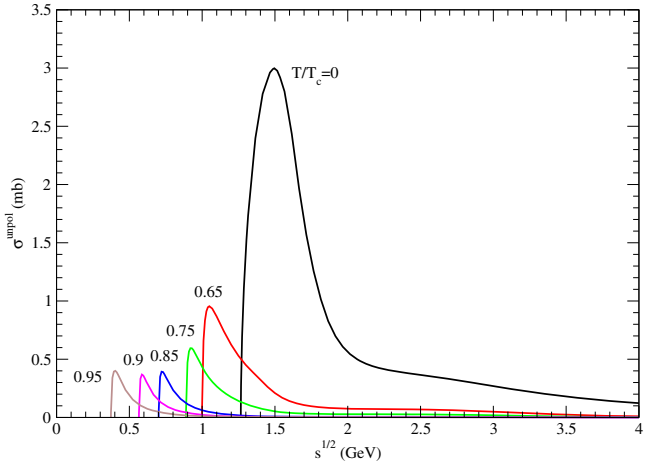

FIG. 3. Cross sections for $\pi K^*\to\rho K$ for $I=1/2$ at various temperatures.

Numerical cross sections plotted in Figs. 3–6 are not convenient for use in future. Hence, the numerical cross sections should be parametrized. All the cross sections shown in Figs. 3–6 approach zero at $\sqrt{s}\to\infty$. In Figs. 3 and 4 every curve exhibits a peak. We may use a function of the form $a_1(\frac{\sqrt{s}-\sqrt{s_0}}{b_1})^{e_1}\exp[e_1(1-\frac{\sqrt{s}-\sqrt{s_0}}{b_1})]$ to fit the numerical cross sections, i.e., the curves. $\sqrt{s_0}$ is the threshold energy and decreases with increasing temperature. The parameters a_1 and b_1 equal the height of the peak and the

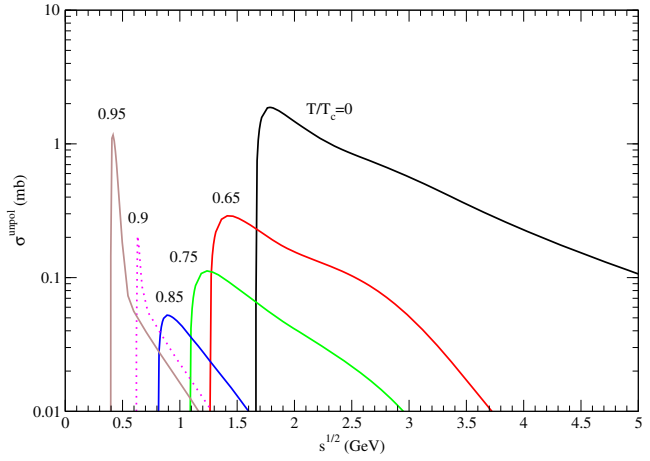

FIG. 4. Cross sections for $\pi K^*\to\rho K^*$ for $I=1/2$ at various temperatures.

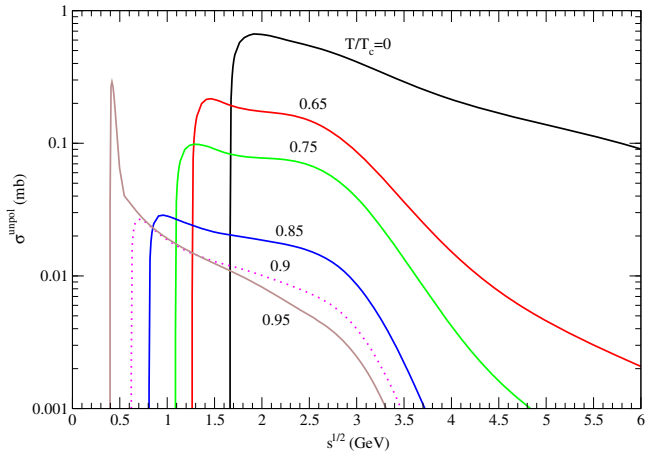

FIG. 5. Cross sections for $\pi K \to \rho K^*$ for $I = 1/2$ at various temperatures.

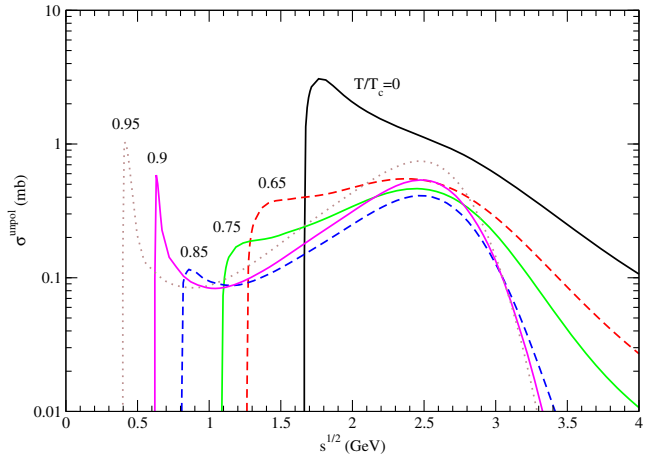

FIG. 6. Cross sections for $\rho K \to \rho K^*$ for $I = 1/2$ at various temperatures.

separation between the peak's location on the $\sqrt{s}$-axis and the threshold energy, respectively. The function has only one maximum and can well fit some curves with one peak, but is insufficient for fitting a curve with two peaks in Fig. 6. To remedy this, we use a sum of two functions,

$$\sigma^{\text{unpol}}(\sqrt{s},T) = a_1\left(\frac{\sqrt{s}-\sqrt{s_0}}{b_1}\right)^{e_1}\exp\left[e_1\left(1-\frac{\sqrt{s}-\sqrt{s_0}}{b_1}\right)\right] + a_2\left(\frac{\sqrt{s}-\sqrt{s_0}}{b_2}\right)^{e_2}\exp\left[e_2\left(1-\frac{\sqrt{s}-\sqrt{s_0}}{b_2}\right)\right], \tag{58}$$

to get a satisfactory fit. No more functions are used because of the terrible computation time. The values of the parameters, a_1, b_1, e_1, a_2, b_2, and e_2, are listed in Table II. The six parameters are positive and depend on temperature. In the table d_0 is the separation between the peak's location on the $\sqrt{s}$-axis and the threshold energy, and $\sqrt{s_z}$ is the square root of the Mandelstam variable at which the cross section is $1/100$ of the peak cross section. At $\sqrt{s} = \sqrt{s_0}$ the parametrization gives zero cross section what is a feature of endothermic reactions. Now a_1 does not equal the peak's height, and the sum of a_1 and a_2 is mainly determined by the peak cross section. The peak cross sections of the 4 reactions have the same behavior: from $T/T_c = 0$ to 0.95 each first decreases to a value and then increases from the value. Correspondingly, a_1, a_2, and $a_1 + a_2$ decrease first and then generally increase. The parameters b_1 and b_2 are related to d_0. If $b_1 < b_2$, $\frac{d\sigma^{\text{unpol}}}{d\sqrt{s}} > 0$ at $\sqrt{s} < b_1$ and $\frac{d\sigma^{\text{unpol}}}{d\sqrt{s}} < 0$ at $\sqrt{s} > b_2$. If $b_1 > b_2$, $\frac{d\sigma^{\text{unpol}}}{d\sqrt{s}} > 0$ at $\sqrt{s} < b_2$ and $\frac{d\sigma^{\text{unpol}}}{d\sqrt{s}} < 0$ at $\sqrt{s} > b_1$.

Space and time are discretized in lattice QCD. Denote the temporal and spatial lattice spacings by a_τ and a_σ, respectively. The temporal extent N_τ satisfies $N_\tau a_\tau = \beta \equiv 1/\mathrm{T}$. Let $x = (\vec{x}, x_4)$ label the space-time lattice sites. With the link variables $U_\mu(\vec{x}, x_4)$ [39] the Polyakov loop at the spatial lattice site $\vec{x}$ is defined as

$$L(\vec{x}) = \mathrm{Tr}\prod_{x_4=1}^{N_\tau} U_4(\vec{x}, x_4). \tag{59}$$

The Polyakov loop correlation function is given by [38]

$$\langle L(\vec{x}_a)L^+(\vec{x}_b)\rangle = \frac{\int\prod_{x\mu}dU_\mu(x)e^{-\beta S_G}L(\vec{x}_a)L^+(\vec{x}_b)\prod_{q=1}^{n_f}(\int\prod_x d\bar{\chi}_x d\chi_x e^{-S_F})^{1/4}}{\int\prod_{x\mu}dU_\mu(x)e^{-\beta S_G}\prod_{q=1}^{n_f}(\int\prod_x d\bar{\chi}_x d\chi_x e^{-S_F})^{1/4}}, \tag{60}$$

where χ_x is the transformed quark field [39], S_G is the gauge action [38], S_F is the staggered fermion action [38], and n_f is the number of dynamical-quark flavors. The temperature dependence of the Polyakov loop correlation function comes from the following two aspects. The first one is that β explicitly gives rise to temperature dependence through a_τ, $e^{-\beta S_G}$, and the two Polyakov loops. The gluon field is subject to the periodic boundary condition that its values at $x_4 = 0$ and $x_4 = N_\tau$ are equal. The quark field satisfies the antiperiodic boundary condition that its values at $x_4 = 0$ and $x_4 = N_\tau$ differ only in sign. The second is that the two boundary conditions give rise to temperature dependence of the gluon field, the quark field, the link variable, and the integration measure.

TABLE II. Values of the parameters. a_1 and a_2 are in units of millibarns; b_1, b_2, d_0, and $\sqrt{s_z}$ are in units of GeV; e_1 and e_2 are dimensionless.

Reactions	T/T_c	a_1	b_1	e_1	a_2	b_2	e_2	d_0	$\sqrt{s_z}$
$I=\frac{1}{2}\pi K^*\to\rho K$	0	1.09	0.25	3.8	1.99	0.14	0.55	0.23	6.57
	0.65	0.37	0.03	0.52	0.68	0.1	0.48	0.05	4.02
	0.75	0.32	0.026	0.57	0.33	0.08	0.42	0.03	3.63
	0.85	0.18	0.017	0.62	0.24	0.047	0.41	0.02	2.9
	0.9	0.17	0.055	0.5	0.23	0.016	0.5	0.02	1.56
	0.95	0.15	0.071	0.64	0.29	0.02	0.47	0.03	1.35
$I=\frac{1}{2}\pi K^*\to\rho K^*$	0	0.94	0.39	0.44	1.13	0.1	0.64	0.12	6.97
	0.65	0.183	0.1	0.5	0.151	0.5	0.8	0.15	4.26
	0.75	0.044	0.107	0.74	0.072	0.259	0.44	0.15	3.77
	0.85	0.017	0.05	0.55	0.038	0.14	0.46	0.08	2.48
	0.9	0.054	0.046	0.16	0.15	0.011	0.71	0.01	1.74
	0.95	0.25	0.005	0.29	1	0.021	0.74	0.02	1.11
$I=\frac{1}{2}\pi K\to\rho K^*$	0	0.34	0.95	0.76	0.5	0.19	0.51	0.25	9.63
	0.65	0.21	0.17	0.53	0.13	1.09	3.9	0.2	5.94
	0.75	0.051	1.34	6.8	0.102	0.22	0.5	0.2	4.85
	0.85	0.016	1.33	4.1	0.03	0.16	0.47	0.15	4.05
	0.9	0.014	0.52	0.51	0.02	0.06	0.45	0.1	3.78
	0.95	0.02	0.013	0.7	0.27	0.018	0.5	0.02	2.92
$I=\frac{1}{2}\rho K\to\rho K^*$	0	1.59	0.08	0.76	1.69	0.26	0.4	0.1	5.02
	0.65	0.37	1.19	7.9	0.4	0.29	0.5	1.1	5.05
	0.75	0.2	0.25	0.48	0.39	1.31	6.9	1.35	4.48
	0.85	0.12	0.08	0.37	0.35	1.79	3.6	1.65	3.55
	0.9	0.58	0.01	0.32	0.538	1.85	15	1.85	3.38
	0.95	1.03	0.019	0.483	0.744	2.07	16	2.05	3.29

Place a heavy quark at $\vec{x}_a$ and a heavy antiquark at $\vec{x}_b$. The Polyakov loop correlation function is related to the free energy $F(T,r)$ of the heavy quark-antiquark pair by

$$-T\ln\langle L(\vec{x}_a)L^+(\vec{x}_b)\rangle = F(T,r)+C', \tag{61}$$

where $r=a_\sigma|\vec{x}_a-\vec{x}_b|$, and C' is a normalization constant. In hadronic matter, i.e., $T<T_c$ the quark-antiquark free energy can be taken as the quark-antiquark potential [40–45]. The lattice gauge calculations in Ref. [38] thus provide the numerical quark-antiquark potential at $r>0.3$ fm at $T/T_c>0.55$. The potential is temperature-dependent and spin-independent. At long distances the potential becomes a distance-independent value. With increasing temperature the value decreases.

The potential between constituents a and b in coordinate space is

$$\begin{aligned}V_{ab}(\vec{r}) =& -\frac{\vec{\lambda}_a}{2}\cdot\frac{\vec{\lambda}_b}{2}\frac{3}{4}D\left[1.3-\left(\frac{T}{T_c}\right)^4\right]\tanh(Ar)\\ &+\frac{\vec{\lambda}_a}{2}\cdot\frac{\vec{\lambda}_b}{2}\frac{6\pi}{25}\frac{v(\lambda r)}{r}\exp(-Er)\\ &-\frac{\vec{\lambda}_a}{2}\cdot\frac{\vec{\lambda}_b}{2}\frac{16\pi^2}{25}\frac{d^3}{\pi^{3/2}}\exp(-d^2r^2)\frac{\vec{s}_a\cdot\vec{s}_b}{m_am_b}\\ &+\frac{\vec{\lambda}_a}{2}\cdot\frac{\vec{\lambda}_b}{2}\frac{4\pi}{25}\frac{1}{r}\frac{d^2v(\lambda r)}{dr^2}\frac{\vec{s}_a\cdot\vec{s}_b}{m_am_b},\end{aligned} \tag{62}$$

where $D=0.7$ GeV, $E=0.6$ GeV, $A=1.5[0.75+0.25(T/T_c)^{10}]^6$ GeV, $\lambda=\sqrt{25/16\pi^2\alpha'}$ with $\alpha'=1.04$ GeV^{-2}, λ_a are the Gell-Mann matrices for the color generators of constituent a, $\vec{s}_a$ is the spin of constituent a, the function v is given by Buchmüller and Tye in Ref. [46], and the quantity d given in Ref. [22] is related to the constituent masses. The temperature dependence of the potential is shown by the first term. The sum of the first and second terms fits the lattice QCD results at intermediate and long distances at $T/T_c>0.55$ [38]. Solving the Schrödinger equation with the quark potential, we obtain the temperature dependence of meson masses and quark-antiquark relative-motion wave functions. The temperature-dependent masses lead to temperature dependence of the threshold energy which is the sum of the masses of the two final mesons for the 2-to-2 reactions or the mass of the final meson for the 2-to-1 reactions. The temperature dependence of the potential, the meson masses, and the mesonic quark-antiquark wave functions bring about the temperature dependence of the unpolarized cross sections for the 2-to-2 reactions via the transition amplitudes in Eqs. (1)–(4), while the masses and wave functions also do this for the 2-to-1 reactions via the transition amplitudes in Eqs. (36)–(39). We note that the transition potentials in Eqs. (54)–(55) are temperature-independent.

The four reactions are endothermic. The cross section for $\pi K^*\to\rho K$ for $I=1/2$ at a given temperature increases

TABLE III. Isospin-averaged unpolarized cross sections versus T/T_c.

$\frac{T}{T_c}$	0	0.6	0.65	0.68	0.7	0.72	0.75	0.78
$\sigma^{un}_{\pi\pi\to\rho}$ (mb)	80.07	54.6	46.93	41.51	37.52	33.28	26.59	19.82
$\sigma^{un}_{\pi K\to K^*}$ (mb)	60.5	42.53	38.79	34.97	31.27	26.79	19.66	15.39
$\frac{T}{T_c}$	0.8	0.82	0.85	0.88	0.9	0.92	0.95	0.99
$\sigma^{un}_{\pi\pi\to\rho}$ (mb)	15.94	13.98	12.37	11.43	10.93	10.18	7.62	0.85
$\sigma^{un}_{\pi K\to K^*}$ (mb)	13.73	12.29	10.74	9.82	9.36	8.69	6.43	0.41

very rapidly from threshold, reaches a maximum, and then decreases rapidly. However, the cross section for $\pi K \to \rho K^*$ for $I = 1/2$ at $T/T_c = 0$, 0.65, 0.75, or 0.85 decreases slowly from its maximum; the cross section for $\rho K \to \rho K^*$ for $I = 1/2$ at $T/T_c = 0.85$ even decreases first and then increases. The cross section for $\rho K \to \rho K^*$ for $I = 1/2$ at $T/T_c = 0.9$ or 0.95 has a narrow peak near threshold and a wide peak around $\sqrt{s} = 2.5$ GeV.

The reaction $\pi K^* \to \rho K$ for $I = 3/2$ is governed by quark interchange only [21]. The flavor matrix element of $\pi K^* \to \rho K$ for $I = 3/2$ is 1, while the one of $\pi K^* \to \rho K$ for $I = 1/2$ due to quark interchange is $-1/2$. The peak cross section of $\pi K^* \to \rho K$ for $I = 3/2$ at $T/T_c = 0.95$ is roughly four times the one of $\pi K^* \to \rho K$ for $I = 1/2$ at the same temperature. Therefore, near the critical temperature quark interchange dominates the reaction $\pi K^* \to \rho K$ for $I = 1/2$. This conclusion can also be drawn in the cases of $\pi K^* \to \rho K^*$, $\pi K \to \rho K^*$, and $\rho K \to \rho K^*$.

The Buchmüller-Tye potential arises from one-gluon exchange plus perturbative one- and two-loop corrections [46], and provides $g_s = \frac{2\sqrt{6\pi}}{5}$ for one-gluon exchange. Set $h = 1/(53\sqrt{\pi})$ fm^{-1}. According to Eq. (43) we calculate isospin-averaged unpolarized cross sections for $\pi\pi \to \rho$ and $\pi K \to K^*$ at various temperatures. Results are listed in Table III. $\sigma^{\rm unpol}$ in Eq. (58) decreases when $\sqrt{s} - \sqrt{s_0}$ increases from the larger one of b_1 and b_2. It is shown in Table III that the cross sections decrease when temperature increases. We thus use the right-hand side of Eq. (58) to fit the numerical cross sections in Table III by replacing $\sqrt{s} - \sqrt{s_0}$ with $T/T_c - 0.42$ for $\pi\pi \to \rho$ or $T/T_c - 0.5$ for $\pi K \to K^*$. In the temperature region $0.6T_c < T < T_c$ hadronic matter exists. The isospin-averaged unpolarized cross section for $\pi\pi \to \rho$ for $0.6T_c \le T < T_c$ is parametrized as

$$\sigma^{\rm un}(T) = 54.1\left(\frac{T/T_c - 0.42}{0.18}\right)^{3.3}\exp\left[3.3\left(1 - \frac{T/T_c - 0.42}{0.18}\right)\right] + 5.32\left(\frac{T/T_c - 0.42}{0.5}\right)^{84}\exp\left[84\left(1 - \frac{T/T_c - 0.42}{0.5}\right)\right], \quad (63)$$

and for $\pi K \to K^*$,

$$\sigma^{\rm un}(T) = 42.2\left(\frac{T/T_c - 0.5}{0.115}\right)^{1.83}\exp\left[1.83\left(1 - \frac{T/T_c - 0.5}{0.115}\right)\right] + 4.95\left(\frac{T/T_c - 0.5}{0.407}\right)^{50}\exp\left[50\left(1 - \frac{T/T_c - 0.5}{0.407}\right)\right]. \quad (64)$$

At $T = 0$ the cross sections for $\pi\pi \to \rho$ and $\pi K \to K^*$ are 80.07 mb and 60.5 mb in comparison with the measured value 80 mb [25] and the estimate 60 mb formed in Ref. [26], respectively. The value 80.07 mb (60.5 mb) is much larger than 0.64 mb (0.27 mb) which is the maximum of the isospin-averaged unpolarized cross section for $\pi\pi \to \rho\rho$ ($\pi K \to \rho K^*$) at $T = 0$ [21,22]. With increasing temperature the cross section for either reaction shown in Table III decreases. As the temperature increases from zero, the long-distance part of the quark potential V_{ab} gradually becomes a distance-independent and temperature-dependent quantity. As the temperature increases from $0.6T_c$ to T_c, the quantity decreases and confinement becomes weaker and weaker. The weakening confinement with increasing temperature makes combining the final quark and the final antiquark into a meson more difficult, and thus reduces the cross section. At $T/T_c = 0.95$ the cross section for $\pi\pi \to \rho$ ($\pi K \to K^*$) is still much larger than the maximum of the isospin-averaged unpolarized cross section for $\pi\pi \to \rho\rho$ ($\pi K \to \rho K^*$), which is 0.11 mb (0.78 mb) at the same temperature [21,22].

VI. SUMMARY

We have provided cross section formulas for the reactions that are governed by quark interchange as well as quark-antiquark annihilation and creation, and have obtained the temperature dependence of the unpolarized cross sections for $\pi K^* \to \rho K$ for $I = 1/2$, $\pi K^* \to \rho K^*$ for $I = 1/2$, $\pi K \to \rho K^*$ for $I = 1/2$, and $\rho K \to \rho K^*$ for $I = 1/2$. Near threshold quark interchange dominates the four channels near the critical temperature; in the other energy region the quark-antiquark annihilation and creation may dominate the four channels. The numerical cross sections are parametrized for future use in the evolution of hadronic matter.

We have proposed a model to study 2-to-1 meson-meson scattering. The isospin-averaged unpolarized cross section for the scattering has been derived, and the cross section

formulas have been applied to study $\pi\pi \to \rho$ and $\pi K \to K^*$. The reactions contain the process where a quark-antiquark pair annihilates into a gluon and subsequently the gluon is absorbed by a quark or an antiquark. The transition potential of the process is derived from the Feynman rules in perturbative QCD. The transition amplitudes corresponding to the four Feynman diagrams are calculated with the transition potential. The isospin-averaged unpolarized cross sections for the two reactions decrease due to weakening confinement with increasing temperature. The numerical cross sections are parametrized.

ACKNOWLEDGMENTS

This work was supported by the National Natural Science Foundation of China under Grant No. 11175111.

[1] J. Gasser and H. Leutwyler, Ann. Phys. (N.Y.) **158**, 142 (1984); Nucl. Phys. **B250**, 465 (1985).
[2] J. Gasser and U. G. Meissner, Phys. Lett. B **258**, 219 (1991); Nucl. Phys. **B357**, 90 (1991).
[3] I. Bijnens, G. Colangelo, G. Ecker, J. Gasser, and M. E. Sainio, Nucl. Phys. **B508**, 263 (1997).
[4] F. Guerrero and J. A. Oller, Nucl. Phys. **B537**, 459 (1999).
[5] A. G. Nicola and J. Peláez, Phys. Rev. D **65**, 054009 (2002).
[6] S. M. Roy, Phys. Lett. B **36**, 353 (1971); M. R. Pennington and S. D. Protopopescu, Phys. Rev. D **7**, 1429 (1973); B. Ananthanarayan, Phys. Rev. D **58**, 036002 (1998); G. Colangelo, J. Gasser, and H. Leutwyler, Nucl. Phys. **B603**, 125 (2001); R. Kamiński, L. Leśniak, and B. Loiseau, Phys. Lett. B **551**, 241 (2003).
[7] T. N. Truong, Phys. Rev. Lett. **61**, 2526 (1988); A. Dobado, M. J. Herrero, and T. N. Truong, Phys. Lett. B **235**, 134 (1990); S. Willenbrock, Phys. Rev. D **43**, 1710 (1991); G.-Y. Qin, W. Z. Deng, Z. G. Xiao, and H. Q. Zheng, Phys. Lett. B **542**, 89 (2002).
[8] T. N. Truong, Phys. Rev. Lett. **67**, 2260 (1991); T. Hannah, Phys. Rev. D **55**, 5613 (1997); A. Dobado and J. R. Peláez, Phys. Rev. D **56**, 3057 (1997); M. Boglione and M. R. Pennington, Z. Phys. C **75**, 113 (1997); J. A. Oller, E. Oset, and J. R. Peláez, Phys. Rev. D **59**, 074001 (1999); J. Nieves, M. P. Valderrama, and E. R. Arriola, Phys. Rev. D **65**, 036002 (2002); J. Nebreda and J. R. Peláez, Phys. Rev. D **81**, 054035 (2010); M. Döring and U.-G. Meißner, J. High Energy Phys. 01 (**2012**) 009.
[9] A. Dobado and J. R. Peláez, Phys. Lett. B **286**, 136 (1992); A. Dobado and J. Morales, Phys. Rev. D **52**, 2878 (1995).
[10] B. S. Zou and D. V. Bugg, Phys. Rev. D **50**, 591 (1994); L. Li, B. S. Zou, and G.-L. Li, Phys. Rev. D **67**, 034025 (2003); F. Q. Wu, B. S. Zou, L. Li, and D. V. Bugg, Nucl. Phys. **A735**, 111 (2004).
[11] J. V. Steele, H. Yamagishi, and I. Zahed, Nucl. Phys. **A615**, 305 (1997).
[12] J. S. Borges, J. S. Barbosa, and V. Oguri, Phys. Lett. B **393**, 413 (1997); **412**, 389 (1997).
[13] J. A. Oller and E. Oset, Nucl. Phys. **A620**, 438 (1997); F.-K. Guo, R.-G. Ping, P.-N. Shen, H.-C. Chiang, and B. S. Zou, Nucl. Phys. **A773**, 78 (2006); I. V. Danilkin, L. I. R. Gil, and M. F. M. Lutz, Phys. Lett. B **703**, 504 (2011); Z.-H. Guo, L. Liu, U.-G. Meißner, J. A. Oller, and A. Rusetsky, Phys. Rev. D **95**, 054004 (2017).
[14] J. A. Oller and E. Oset, Phys. Rev. D **60**, 074023 (1999); M. Albaladejo, J. A. Oller, and L. Roca, Phys. Rev. D **82**, 094019 (2010).
[15] J. Nieves and E. R. Arriola, Phys. Lett. B **455**, 30 (1999); M. Albaladejo, J. A. Oller, E. Oset, G. Rios, and L. Roca, J. High Energy Phys. 08 (**2012**) 071.
[16] G. Janssen, B. C. Pearce, K. Holinde, and J. Speth, Phys. Rev. D **52**, 2690 (1995).
[17] B. A. Li, Phys. Rev. D **52**, 5165 (1995); B. A. Li, D.-N. Gao, and M.-L. Yan, Phys. Rev. D **58**, 094031 (1998).
[18] D. Black, A. H. Fariborz, and J. Schechter, Phys. Rev. D **61**, 074030 (2000).
[19] T. Barnes and E. S. Swanson, Phys. Rev. D **46**, 131 (1992); E. S. Swanson, Ann. Phys. (N.Y.) **220**, 73 (1992); T. Barnes, E. S. Swanson, and J. Weinstein, Phys. Rev. D **46**, 4868 (1992); T. Barnes, N. Black, and E. S. Swanson, Phys. Rev. C **63**, 025204 (2001).
[20] Y.-Q. Li and X.-M. Xu, Nucl. Phys. **A794**, 210 (2007).
[21] Z.-Y. Shen and X.-M. Xu, J. Korean Phys. Soc. **66**, 754 (2015).
[22] Z.-Y. Shen, X.-M. Xu, and H. J. Weber, Phys. Rev. D **94**, 034030 (2016).
[23] D. Lohse, J. W. Durso, K. Holinde, and J. Speth, Nucl. Phys. **A516**, 513 (1990).
[24] G. E. Brown, C. M. Ko, Z. G. Wu, and L. H. Xia, Phys. Rev. C **43**, 1881 (1991).
[25] V. Flaminio, W. G. Moorhead, D. R. O. Morrison, and N. Rivoire, CERN, Geneva Report No. CERN-HERA-84-01, 1984.
[26] C. M. Ko, Phys. Rev. C **23**, 2760 (1981).
[27] H. Hellmann, *Einführung in die Quantenchemie* (Deuticke, Leipzig und Wien, 1937); R. P. Feynman, Phys. Rev. **56**, 340 (1939).
[28] J. Ruiz de Elvira, U.-G. Meißner, A. Rusetsky, and G. Schierholz, Eur. Phys. J. C **77**, 659 (2017).
[29] J. Weinstein and N. Isgur, Phys. Rev. D **41**, 2236 (1990).
[30] S.-T. Ji, Z.-Y. Shen, and X.-M. Xu, J. Phys. G **42**, 095110 (2015).
[31] K. Nakamura *et al.* (Particle Data Group), J. Phys. G **37**, 075021 (2010).
[32] E. Colton, E. Malamud, P. E. Schlein, A. D. Johnson, V. J. Stenger, and P. G. Wohlmut, Phys. Rev. D **3**, 2028 (1971); N. B. Durusoy, M. Baubillier, R. George, M. Goldberg, A. M. Touchard, N. Armenise, M. T. Fogli-Muciaccia, and A. Silvestri, Phys. Lett. B **45**, 517 (1973); M. J. Losty, V. Chaloupka, A. Ferrando, L. Montanet, E. Paul, D. Yaffe,

A. Zieminski, J. Alitti, B. Gandois, and J. Louie, Nucl. Phys. **B69**, 185 (1974); W. Hoogland *et al.*, Nucl. Phys. **B126**, 109 (1977).

[33] S. D. Protopopescu, M. Alston-Garnjost, A. Barbaro-Galtieri, S. M. Flatté, J. H. Friedman, T. A. Lasinski, G. R. Lynch, M. S. Rabin, and F. T. Solmitz, Phys. Rev. D **7**, 1279 (1973); B. Hyams *et al.*, Nucl. Phys. **B64**, 134 (1973); P. Estabrooks and A. D. Martin, Nucl. Phys. **B79**, 301 (1974); V. Srinivasan *et al.*, Phys. Rev. D **12**, 681 (1975); L. Rosselet *et al.*, Phys. Rev. D **15**, 574 (1977); C. D. Froggatt and J. L. Petersen, Nucl. Phys. **B129**, 89 (1977); A. A. Bel'kov, S. A. Bunyatov, K. N. Mukhin, O. O. Patarakin, V. M. Sidorov, M. M. Sulkovskaya, A. F. Sustavov, and V. A. Yarba, JETP Lett. **29**, 597 (1979); E. A. Alekseeva, A. A. Kartamyshev, V. K. Makar'in, K. N. Mukhin, O. O. Patarakin, M. M. Sulkovskaya, A. F. Sustavov, L. V. Surkova, and L. A. Chernysheva, Sov. Phys. JETP **55**, 591 (1982); R. García-Martín, R. Kamiński, J. R. Peláez, J. R. de Elvira, and F. J. Ynduráin, Phys. Rev. D **83**, 074004 (2011).

[34] M. Kohno and W. Weise, Nucl. Phys. **A454**, 429 (1986); **A479**, 433 (1988).

[35] T. Muta, *Foundations of Quantum Chromodynamics* (World Scientific, Singapore, 1987).

[36] J. D. Bjorken and S. D. Drell, *Relativistic Quantum Mechanics* (McGraw-Hill, New York, 1964).

[37] S. Gupta, X. Luo, B. Mohanty, H. G. Ritter, and N. Xu, Science **332**, 1525 (2011).

[38] F. Karsch, E. Laermann, and A. Peikert, Nucl. Phys. **B605**, 579 (2001).

[39] H. J. Rothe, *Lattice Gauge Theories* (World Scientific, Singapore, 1997).

[40] A. Rothkopf, T. Hatsuda, and S. Sasaki, Phys. Rev. Lett. **108**, 162001 (2012); Y. Burnier and A. Rothkopf, Phys. Rev. Lett. **111**, 182003 (2013).

[41] Y. Burnier, O. Kaczmarek, and A. Rothkopf, *Proc. Sci.*, LATTICE2014 (2015) 220 [arXiv:1410.7311].

[42] Y. Burnier, O. Kaczmarek, and A. Rothkopf, J. High Energy Phys. 12 (2015) 101.

[43] Y. Burnier and A. Rothkopf, Phys. Rev. D **95**, 054511 (2017).

[44] S. H. Lee, K. Morita, T. Song, and C. M. Ko, Phys. Rev. D **89**, 094015 (2014).

[45] Z.-Y. Shen and X.-M. Xu, Chin. Phys. C **39**, 074103 (2015).

[46] W. Buchmüller and S.-H. H. Tye, Phys. Rev. D **24**, 132 (1981).